Proceedings of IMECE2005
2005 ASME International Mechanical Engineering Congress and Exposition
November 5-11, 2005, Orlando, Florida USA

IMECE2005-81435

DEMONSTRATION AND CHARACTERIZATION OF A MULTI-STAGE SILICON MICROTURBINE

Changgu Lee[1], Luc G. Fréchette[2,1]
[1]Columbia University, Dept. of Mech. Eng. New York, NY 10027, U.S.A.
[2]Université de Sherbrooke, Dept. of Mech. Eng., Sherbrooke, QC, J1K 2R1, Canada

Abstract - This paper presents the experimental testing and characterization of a microscale radial outflow turbine with four concentric stages. The device is a five layer structure composed of shallow and deep reactive ion etched silicon wafers and an ultrasonically drilled Pyrex glass wafer that are assembled using anodic and fusion bonding techniques. They enclose a 4mm diameter rotor that was spun up to 330,000 rpm and produced roughly 0.1W of mechanical power from each stage totaling 0.38W with 0.75 atm differential pressure across the microturbine. Modeling of the turbine based on a mean line analysis with loss correlations extracted from CFD suggests a turbine isentropic efficiency of 35% and Re=266 at the maximum speed. The pressure distribution across the blades rows was measured and showed close agreement with the calculation results. Using the model, the microturbine is predicted to produce 3.2 watts with an isentropic efficiency of 63% at a rotor speed of 1.1 million rpm.

INTRODUCTION

Recently, MEMS-based silicon turbomachines have been developed for various applications, such as power generation, propulsion, compression, and pumping [1], [2]. Although there are limitations in the choice of structural shapes due to the 2D characteristic of the microfabrication process, the potential benefits of high power per unit volume and low production cost due to batch processing are attractive [3], [4]. To date, the development efforts of micro-scale turbomachines have mostly focused on those with just one pair of stator and rotor blade rows. However, a single stage configuration can only provide a limited pressure ratio, consequently restricting the thermal efficiency of miniature thermodynamic machines. Thus the need for multiple blade rows has arisen from theoretical and practical aspects during the development of gas turbines [1] and steam turbines [5]. High pressure ratios are especially beneficial to achieve a reasonable efficiency in a Rankine cycle, which produces power by expanding high pressure, superheated steam through a turbine. The working fluid is pressurized in liquid state by a pump, allowing high pressure ratios, which compensate for lower operating temperatures compared to gas phase Brayton power cycles.

In this context, the concept of a multi-stage turbine was suggested for miniature Rankine cycle power generation [5]. The whole system consists of microfabricated heat exchangers, a pump, a generator, bearings, and the turbine. The system was designed to generate a few watts of electrical power from a source of heat with an overall energy conversion efficiency between 1-12%, depending on the thermal conditions. As a core power conversion component, the turbine was analyzed and designed to produce several watts of mechanical power with an isentropic efficiency of 60-70% at the design operating conditions.

This paper will present testing and characterization of the demo turbine device to demonstrate the concept of the multi-stage turbine and to develop related technologies. The device was designed to have four stages of blade rows producing about 1 watt of mechanical power each at 1.3 million RPM from pressurized steam, which corresponds to 270m/s of rotor tip speed.

In the first part of this paper, the configuration of the device and the working principle of the components will be shown briefly. Then the fabrication process of the five-layer structure using silicon bulk micromachining techniques will be described. The characterization and test results of the rotating system will be presented, with a focus on the microturbine performance.

DEVICE CONFIGURATION

The overall configuration consists of five micromachined layers that enclose a 4 mm diameter rotor and form the flow paths to the bearings and turbine, as shown in Figure 1. The bearing system, which supports the rotor axially and laterally as it rotates, is composed of hydrostatic thrust and journal bearings. The rotor is a 4mm diameter disk with four concentric blade rows on one side, each composed of 80 to 180 blades. Four rows of stator blades also extend out from the upper layer, between the rotor blade rows, making an

interdigitated radial flow turbine. The height of the rotor blades is 70um, and that of the stator blades is 50um.

As illustrated in Figure 1, the high pressure flow is fed from the top, does a right angle turn into the first blade row and flows outward through the turbine. Expansion of the working fluid provides the energy to drive the rotor. The increasing flow area along the stages maintains a nearly constant flow velocity which can prevent premature choking in the flow passages.

The profile details of the fabricated blades and their shapes are described in Table 1 and Figure 2 respectively. The geometry chosen for this study is based on the NACA A3K7 turbine airfoil [6]. The primary series A3K7 is for reaction blades in which there is acceleration through the cascades. The solidity of each blade row (chord-to-pitch ratio) is 2, and the radial gap between the blade rows is 25um. The base tip clearance of the rotor blade is 1.5um.

The journal bearing, which is a circular gap of 20um wide and 400um deep, surrounds the rotor to support it radially. The thrust bearing, which has a 1 um gap, is located on the bottom side of the rotor. It consists of 34 nozzles, which are 10 um diameter and 85 um long.

The type of bearing system is directly inspired from previous microturbines [7]. The journal bearing exploits the boundary growth at the entrance of the narrow channel and difference of pressure distribution between opposite sides of the bearing to create a restoring force. The thrust bearing utilizes the flow resistances between nozzles and a planar clearance to balance out the axial movement of the rotor. However, unlike the previous thrust bearings, which had nozzles on top and bottom sides to axially center the rotor, the current device has only bottom side nozzles that act against the turbine pressure.

The whole device chip set is composed of three pieces, as shown in Figure 1. The top piece, which is the stack of layers A and B, has the turbine inlet and outlet flow channels and the stator blades. The rotor includes protrusions (noted as "speed bumps") to facilitate measurement of rotational speed. The bottom piece, which is the stack of layers C, D, and E, is the structure for the bearing system and related flow channels. In the fabrication process, the top and bottom pieces are made separately, with the rotor fabricated as part of layer C. It is released from layer C when the journal bearing etch is completed and is then assembled manually before testing, as illustrated in Figure 1(c).

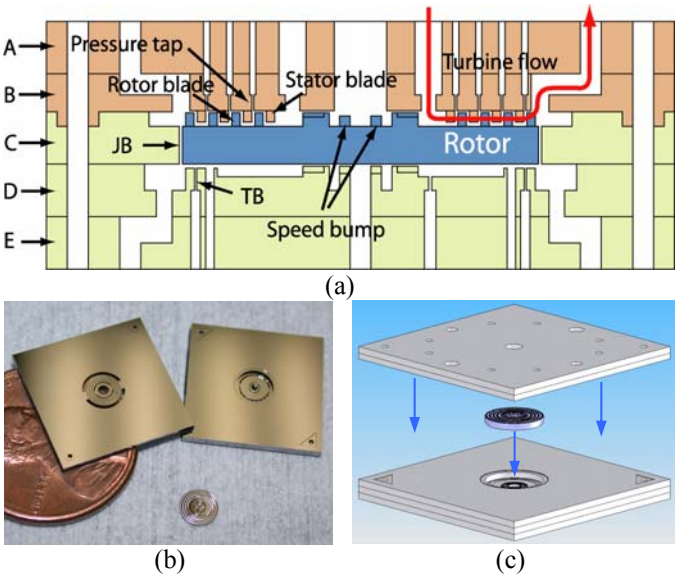

Figure 1 – Configuration and assembly of the device: (a) schematic of the device; (b) picture of three pieces; (c) 3D schematic of chip assembly.

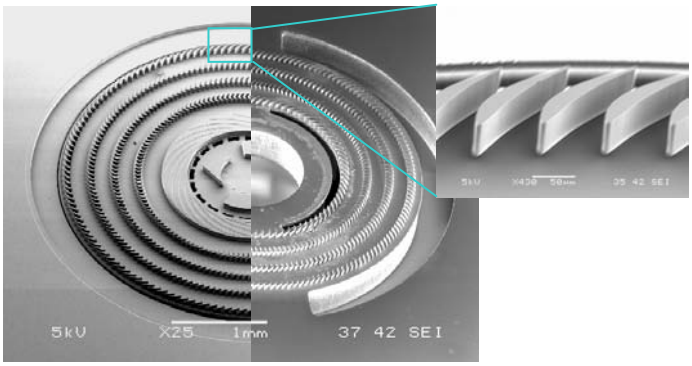

Figure 2 – Microturbine rotor and stator: left side is the rotor and right side is the stator. Zoom in picture shows the characteristic 2D shape of micromachined blades using DRIE.

Table 1 – Specification of the stator and rotor blades rows.

Stator					
Stage	Inlet angle(°)	Outlet angle(°)	Radial length(um)	Chord length(um)	No. of blades
1	14	67	96.4	140.8	87
2	53	66	93.3	98	155
3	33	61	93.4	96.4	168
4	16	59	92	94.2	181
Rotor					
Stage	Inlet angle(°)	Outlet angle(°)	Radial length(um)	Chord length(um)	No. of blades
1	53	70	94.1	98.9	139
2	37	62	93.8	106.9	158
3	16	57	92.2	116.3	168
4	-9	65	90.3	147.6	152

MICROFABRICATION

The complete device is composed of the five layers illustrated in Figure 3: one Pyrex glass wafer, one silicon-on-insulator (SOI) and three silicon wafers.

The glass wafer is 500um thick, and the other wafers are 450um thick. The glass wafer, which is the first layer, was machined by ultrasonic drilling. The SOI wafer corresponding to layer B consists of two layers of silicon (400um and 50um thick), separated by 0.5 micron of silicon oxide. On the thick side of the wafer, the channels for turbine flow and pressure measurement taps are patterned and etched using deep reactive ion etching (DRIE). On the thinner side, the stator blades are also formed using the DRIE process. Layer C, which includes the rotor, is etched from the top side first to form the rotor blades and an oxide layer of 1.5um is deposited as an etch stop. By etching the journal bearing through the wafer from the other side, the rotor is cut out and separated from layer C. Layer D goes through a few shallow etch steps using reactive ion etching (RIE) with depths ranging from 0.5 to 6 um. Then it is etched halfway through from both sides using DRIE to form holes and connecting channels. Similarly, layer E is etched from each side using the DRIE process, also forming flow channels as well as inlet and outlet holes for supply and exhaust of the bearing flows.

The machined layers A and B are anodically bonded at 1000V and 350°C, while layers C, D, and E are fusion-bonded under high pressure (216kPa) and annealed at 1100°C for 1 hour in a nitrogen environment.

Among the features of the device, the blades were the most fragile since they protruded from the substrate; caution in handling was critical during fabrication. Although the wafers with those features were carefully handled, some of the blades were broken during the bonding and washing processes by gripping them with tweezers. As discussed later, the damage incurred on the blades might affect the performance slightly.

Normally DRIE etching leaves the bottom surface rounded near walls (Figure 4), and narrow features are etched less than large open areas. This may pose a challenge when the rotor and stator blades are interdigitated and the tips approach the etched surface, especially near the walls. Originally the rotor blades were designed to have same height as the stator blades. But considering the etch uniformity problem, 20um of safety margin was given at the stator blade tips. This excessive tip clearance is also expected to adversely affect the turbine performance.

MODELLING

The turbine flow rate and rotational speed are calculated by iteration until the turbine exit pressure matches the given outlet condition and the power produced from the turbine matches the dissipated power by viscous drag in the bearings and other components. To estimate the turbine performance, a mean line analysis based on velocity triangles with loss factors was used [8]. This low order modeling approach is the basis for preliminary design of traditional multi-stage turbomachinery [9].

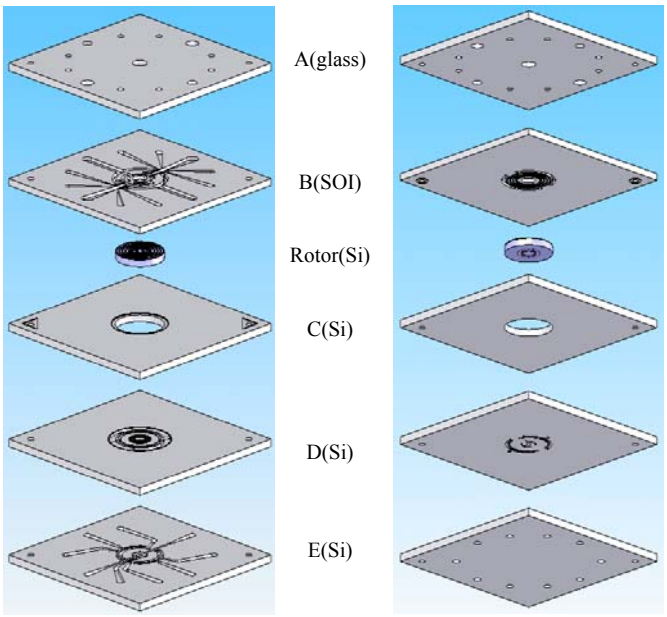

Figure 3 – Exploded view of five layer device.

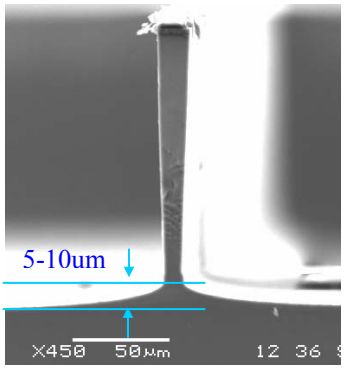

Figure 4 – Non-uniformity of deep etched surface. Uniformity depends on the feature and recipe of DRIE.

The flow is considered to be compressible (ideal gas) and adiabatic. The process consists of conserving total enthalpy across each stator, rothalpy across each rotor, and conserving mass throughout. In this calculation, the static pressures are given as inlet and outlet conditions. A pressure loss coefficient correlation is applied to represent the viscous losses across the blade rows and a blockage coefficient is used to consider the boundary layer growth and changing passage area.

The pressure loss coefficient is used as the turbomachinery loss factor, and is defined as:

$$Y = \frac{P_{01} - P_{02}}{P_{01} - P_2} \qquad (1)$$

where the subscripts represent: 1 inlet, 2 exit, and 0 total (stagnation) conditions. The loss depends on the geometry and flow conditions. For a given loss coefficient, the unknown exit conditions can be defined in the calculation process. The

correlation for the profile loss of the turbine blades was obtained by 2D CFD calculations and expressed as a function of Reynolds number based on boundary layer theory [10] as follows:

$$Y = \frac{C_1}{\sqrt{\mathrm{Re}}} + \frac{C_2}{\mathrm{Re}} \qquad (2)$$

where C_1 and C_2 are functions of geometry, incidence, and Mach number. Based on the CFD data, the impact of incidence and Mach number were found to be relatively small compared to Reynolds number effects. For simplicity here, the constants are considered as functions of geometry only, especially camber angle, assuming negligible incidence effects and low Mach numbers (M<0.2).

The loss may be split into several categories such as profile loss, annulus loss, secondary loss, and tip clearance loss [11]. The correlation mentioned above corresponds to the profile loss which is associated with boundary layer growth over the blade profile, a characteristic of the two-dimensional flow around the airfoil. The other loses are related to 3D effects of the turbine flow. In the current modeling, these 3D effects were not predicted, but were considered by multiplying the profile loss coefficient by a factor greater than unity. This approach assumes that the total loss is proportional to the profile loss, as suggested in large scale turbine research [11] and microscale investigations [12].

Blockage is also a factor that diminishes the performance of turbomachinery. The blockage was defined based on previously published CFD results [12], and boundary layer growth theory as follows:

$$K = 1 - a\sqrt{\Delta r} \qquad (3)$$

where Δr represents radial position from the flow inlet, and the constant "*a*" depends on the geometry and flow condition.

Previous CFD investigations [8] suggest that the exit flow angle remains constant over a wide range of Re and the values were close to the geometric blade angle. Deviation effects were therefore not included in this model.

Considering these loss factors, the isentropic efficiency of the turbine is calculated according to:

$$\eta = \frac{h_{01} - h_{02}}{h_{01} - h_{02s}} \qquad (4)$$

where *h* is enthalpy and the subscript *s* represents isentropic processes. Results of device modeling will be shown along with the experimental results in the next section.

EXPERIMENTAL TESTING AND ANALYSIS OF PERFORMANCE

1) Test setup and operating procedures

The turbine chip mounts in a plexiglass package with o-rings and fluidic pipes to connect the device to a flow handling and measuring system, which consists of mass flow meters, pressure sensors, control valves, data acquisition and control (DAQ) system, and a fiber optic speed sensor.

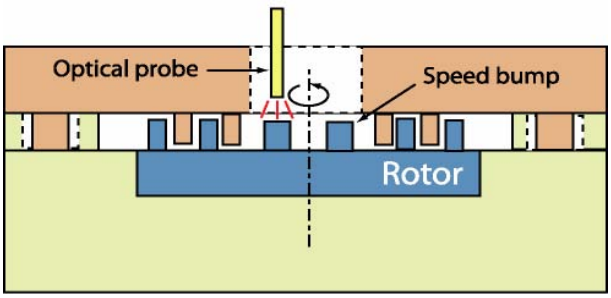

Figure 5 – speed sensing using speed bump and optical probe

For turbine characterization, 8 pressure sensors are connected to inter-blade row static pressure taps, which correspond to the exit points of each blade row (Figure 1). The turbine inlet pressure could not be directly measured due to the lack of space for the pressure tap in the device, but was derived by calibrating the pressure drop in the flow connections and channels feeding the turbine and measuring the upstream pressure.

The rotational speed is measured from the fiber optic speed sensor as shown in Figure 5. While the rotor spins, the optical probe senses the displacement signal from the bumps, which generates a square wave shape that is transferred to the spectrum analyzer of the PC-based DAQ system to get the rotation rate.

The device is operated by maintaining the thrust bearing flow rate constant with a fixed feed pressure. The turbine flow rate is then increased by regulating the differential pressure between the inlet and exit of the turbine.

2) Overall performance

During operation, pressure, flow rate, and rotation rate data were obtained through the DAQ system. Figure 6 shows the turbine flow rate as a function of differential pressure between turbine inlet and exit (*dP*). The uncertainty in flow rate comes from the measurement error of the sensor, which is 1% of full scale measurement. The error on pressure stems from the calibration of the turbine inlet pressure measurement, which is ±5%. The model predictions slightly underestimate the measurements, but are within the error range.

Figure 7 shows the rotational speed in revolutions per minute (rpm) as a function of turbine flow rate. The maximum speed measured from the test was 330,000rpm, which corresponds to 70m/s in tip speed for 4mm diameter rotor. Up to this speed, no instability in the rotor operation was observed. Currently, the rotational speed achieved has mostly been limited by device failures stemming from bearing limitations and mechanical failure.

The model calculates the speed and turbine flow rate using the measured pressure differential as an input. The modeling results show slightly higher values for the same flow rate, compared to the experimental data. As mentioned previously, the model does not include the loss factors for changing incidence and high Mach number, and simply accounts for 3D

losses by applying a correction factor. This may contribute to the higher prediction of the model. Also, the excessive tip clearance of the stator could be a cause. As mentioned, the clearance between the stator blade tips and the overetched rotor surface was about 40% of the blade height. That portion of the turbine flow can pass through the stator blade rows without appropriate turning, which would in turn reduce the fluid-to-mechanical energy conversion in the rotor, hence resulting in lower speed and power per unit flow. Another reason might be the blade damage from the fabrication process and handling of the device. Due to the broken blades, the flow resistance should be lower and the measured flow rate higher than an undamaged turbine. However, the impact of the blade damage on the performance is not expected to be significant because the number of broken blades was only 5-30 out of 1200 for the stator and the rotor, which is relatively small.

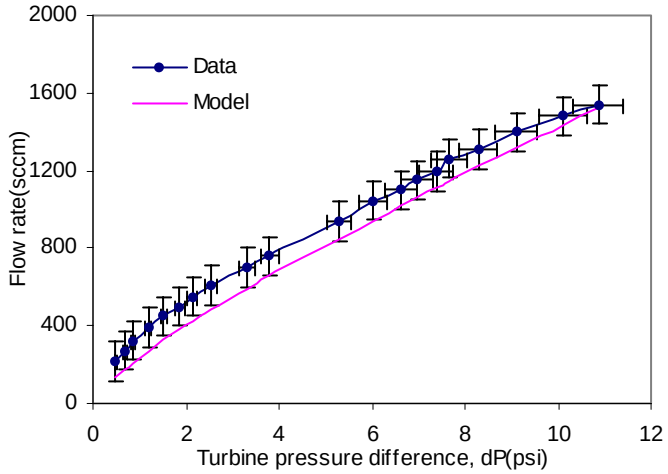

Figure 6 – Flow rate as a function of differential pressure across the multistage microturbine.

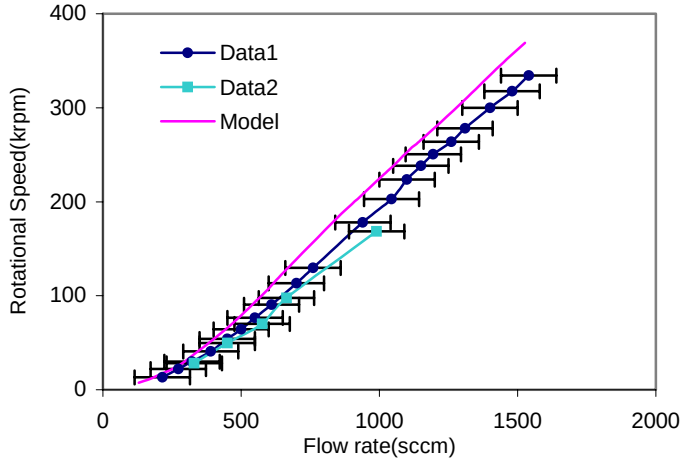

Figure 7 – Rotation rate as a function of air flow rate through the turbine. Data is presented for two different devices showing repeatability.

3) Turbine characterization

The pressures between the blade rows were measured at each operating condition. Figure 8 shows the pressure distribution at one data point. The trend of the other data points is typically similar to that illustrated here. Generally the mechanical power generated by the flow is proportional to the pressure drop across the rotor blades. The calculation reveals that the pressure drop across the 4th rotor blade row is a slightly higher than for the 3rd row, which is reflected by the larger power for the 4th stage compared to the 3rd stage in Figure 9. This is due to the exit flow angle difference between the two rows. The design outlet angle of 3rd rotor blade row is lower by 8 degree than that of the 4th row, as shown in Table 1. Originally, the blade outlet angles were designed to decrease by 5 degrees from stage to stage, but in the final phase of the design process, the gap between the blade rows was increased by cutting off the trailing edge, which modified the original blade angles.

The power produced from each stage is around 0.1 watt in average, totaling 0.38 watt at the highest measured speed.

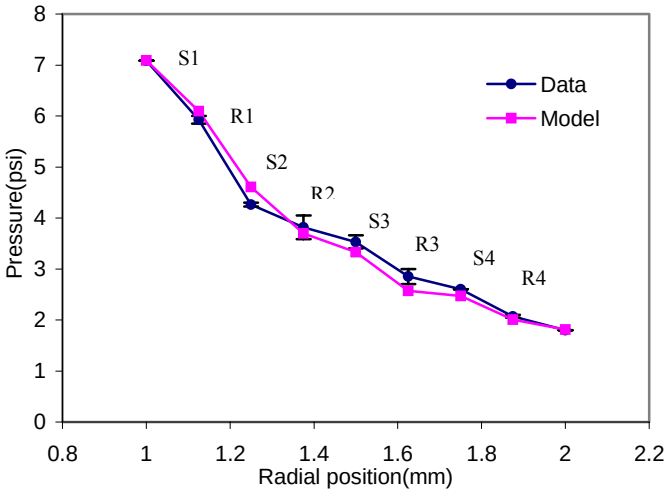

Figure 8 – Pressure distribution throughout the multistage microturbine. Radial position indicates the distance from the center of the rotor. The rotors and stators for each of the 4 stages are identified by R# and S# respectively.

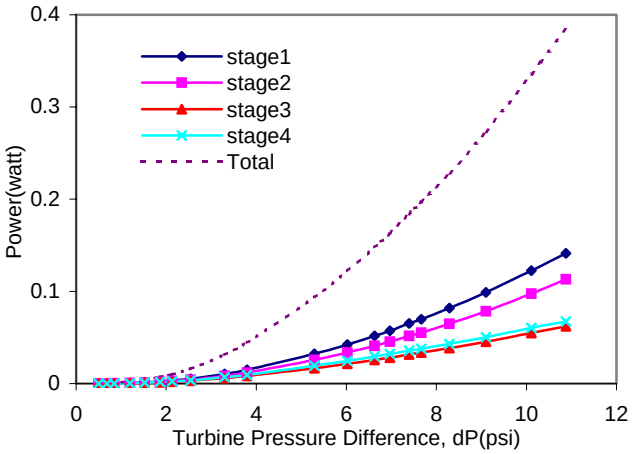

Figure 9 – Power production from each stage

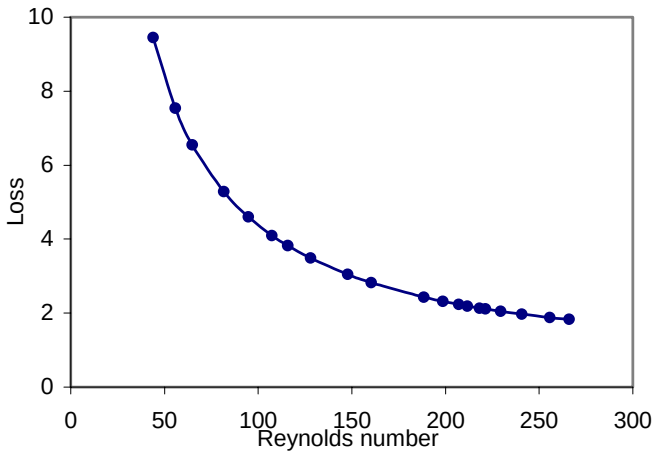

Figure 10 – Pressure loss coefficient as a function of Reynolds number. The numbers are averaged values across the blade rows. Reynolds number is based on blade chord length and inlet properties.

4) Loss and efficiency

Unlike large scale turbomachinery, which operate usually at high Reynolds numbers ($10^6 < Re < 10^8$), this microturbine runs at relatively low Reynolds number, in the range $10^2 < Re < 10^3$. The viscous loss effects are clearly expected to become dominant in the microturbine. The turbine cascade CFD calculation for micro scale turbines showed that the pressure loss is at least one order of magnitude higher than for conventional machines [8], [11]. Figures 10 and 11 show the averaged loss and total isentropic efficiency, respectively, as a function of the averaged Reynolds number for the current geometry and flow condition. As expected, the viscous losses decreases as Re increases, and consequently, the isentropic turbine efficiency increases, reaching 35.7% at Re=266 (Figure 11). These figures reveal the significant impact of the Reynolds number, especially in this low range, and the need for higher speed operation for better efficiency.

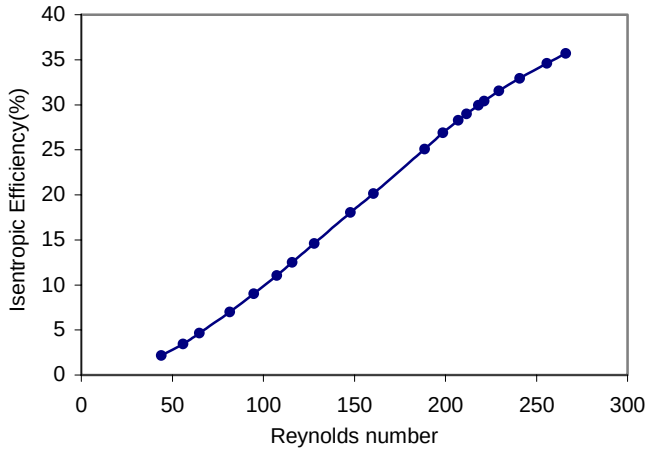

Figure 11 – Total isentropic efficiency of the turbine as a function of Reynolds number.

5) Prediction for higher speed operation

As shown in the previous section, the efficiency at the measured speed is still much lower than that of large scale turbines, which are normally over 80-90%. Although it's not expected that small devices can reach efficiency levels of large machines due to fundamental scaling, it is desirable to increase the turbine efficiency up to a certain level to achieve reasonable performance of the overall power production system.

Figures 12 and 13 show the projected turbine efficiency and the power produced from each stage. In these calculations, the static pressure at the outlet is fixed at atmospheric conditions and the inlet static pressure varies. The speed and flow rate at the highest performance point are 1.1 million rpm and 3500sccm, with a turbine pressure ratio of 3:1. The projected efficiency reaches up to 63% at Re=674 for a total turbine power of 3.2 watts. The estimated efficiency appears to be acceptable considering the micro Rankine power cycle analysis [5]. Therefore, high speed operation over 1 million rpm or Re=600 is recommended for the current design to achieve the required levels of performance.

These predictions suggest that the current multistage turbine configuration may need to be revised, since the power production distribution at high pressure range is different from the low pressure range, as shown in Figure 12. The increasing production of the 2nd stage over the 1st stage comes from higher expansion in that stage. This phenomenon could be undesirable because the unexpected expansion can cause premature choking and deteriorate the overall performance of the turbine. In this perspective, further analysis of blockage, loss and deviation in low Reynolds turbomachinery and high-speed testing seem to be necessary to investigate this problem.

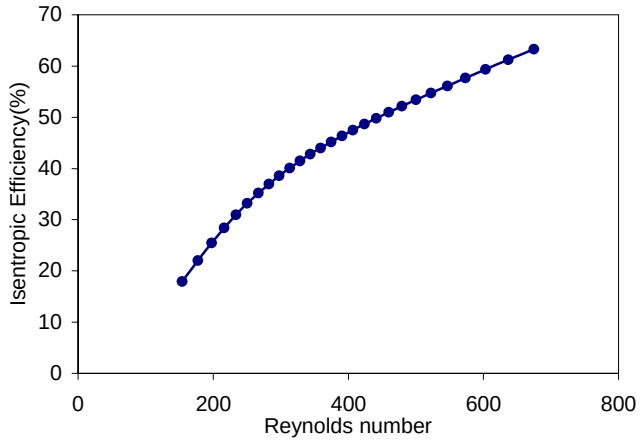

Figure 12 – Total isentropic efficiency at extended Re range

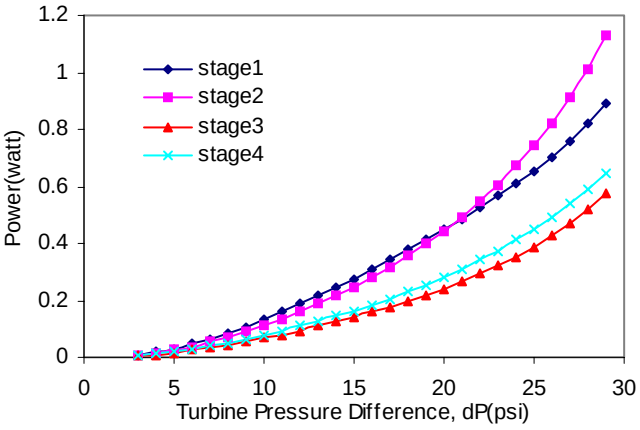

Figure 13 – Predicted power production from each stage at higher differential pressure

CONCLUSION

A silicon microturbine with four concentric stages was fabricated, demonstrated, and characterized. The turbine rotor is supported by gas lubricated bearings and was spun up to 330,000 rpm producing 0.38 watt of mechanical power. The calculation using an analytical model suggests 35% of total isentropic efficiency with an average Re=266 in the turbine. The efficiency at 1.1 million rpm is estimated to reach 63%, producing 3.2 watts of total power at Re=674. The measured speed, flow rate, and pressure distribution between the blade rows show close agreement with the modeling results.

Considering the unprecedented small scale of the blades and low Reynolds numbers, the power production and efficiency level at the recommended operation range is quite encouraging in the perspective of the whole Rankine cycle efficiency. This research is expected to provide a guideline on the smallest size and lowest Reynolds number range for practical microturbines, and contribute to the development of other types of multi-stage micro scale turbomachiery, such as pumps and compressors.

ACKNOWLEDGEMENT

This work was supported by the NASA Glenn Research Center, Alternate Fuels Foundation Technologies program (contracts NAS3-02118 and NAS3-03105), monitored by Dr. Glenn Beheim. The authors gratefully acknowledge this support.

The fabrication work was performed in part at the Cornell NanoScale Science and Technology Facility (CNF), a member of the National Nanotechnology Infrastructure Network, which is supported by the National Science Foundation (Grant ECS 03-35765).

REFERENCE

[1] Epstein A. H. "Millimeter-Scale, Micro-Electro-Mechanical Systems Gas Turbine Engines," *ASME J. of Engineering for Gas Turbines and Power*, vol. 126, pp 205-226, 2004.

[2] Kang, P., Tanaka, S., and Esashi, M. "Demonstration of a MEMS-based Turbocharger," Proc. 4th Int'l Workshop on Micro & Nanotech. for Power Generation & Energy Conversion Appl. (Power MEMS 2004), Kyoto, Japan, Nov. 28-30, 2004.

[3] Epstein A.H. and Senturia S.D., "Macro Power from Micro Machinery", *Science*, **276**, p.1211, 1997.

[4] Epstein, A.H., et al., "Micro-Heat Engines, Gas Turbines, and Rocket Engines - The MIT Microengine Project," AIAA Paper 97-1773, 28th AIAA Fluid Dynamics Conference, Snowmass Village, 1997.

[5] Fréchette, L.G., Lee, C., Arslan, S., Liu, Y.-C., "Design of a Microfabricated Rankine Cycle Steam Turbine for Power Generation", Proc. ASME Int'l Mech. Eng. Congress & Expo., Wash., D.C., Nov. 16-21, 2003.

[6] Dunavant, J. C., and Erwin, J. R., "Investigation of a Related Series of Turbine Blade Profiles in Cascades", NACA Tech. Note 3802, 1956.

[7] Fréchette, L.G., Jacobson, S. A., Ehrich, F.F., Ghodssi, R., Khanna, R., Wong, C.W., Zhang, X., Lin, C.-C., Schmidt, M.A., Epstein, A.H., "High-Speed Microfabricated Silicon Turbomachinery and Fluid Film Bearings". *IEEE/ASME J. Microelectromechanical Systems*, vol. 13, no 6, 2004.

[8] Lee C, Arslan S, Frechette L. G., "Design principles and aerodynamics of low Reynolds number multi-stage microturbomachinery," Proc. ASME Int'l Mech. Eng. Congress & Expo., Wash., D.C., Nov. 13-19, 2004.

[9] Kerrebrock, J.L., *Aircraft Engines and Gas Turbines*, 2nd Ed., The MIT Press, Cambridge, Massachusetts, pp 478, 1992.

[10] Schlichting, H., *Boundary-Layer Theory*, 7th Ed., McGraw Hill, New York, pp 817, 1979.

[11] Horlock, J. H., *Axial flow turbines*, Robert E. Krieger publishing company, 1966

[12] Mehra, A., *Computational Investigation and Design of Low Reynolds Number Micro-Turbomachinery*. S.M. Thesis, Massachusetts Institute of Technology, Cambridge, MA, 1997.